

Stretchable, Washable, and Ultrathin Triboelectric Nanogenerators as Skin-Like Highly Sensitive Self-Powered Haptic Sensors

Yang Jiang, Kai Dong, Xin Li, Jie An, Dequan Wu, Xiao Peng, Jia Yi, Chuan Ning, Renwei Cheng, Pengtao Yu, and Zhong Lin Wang*

Accompanying the boom in multifunctional wearable electronics, flexible, sustainable, and wearable power sources are facing great challenges. Here, a stretchable, washable, and ultrathin skin-inspired triboelectric nanogenerator (SI-TENG) to harvest human motion energy and act as a highly sensitive self-powered haptic sensor is reported. With the optimized material selections and structure design, the SI-TENG is bestowed with some merits, such as stretchability ($\approx 800\%$), ultrathin ($\approx 89 \mu\text{m}$), and light-weight ($\approx 0.23 \text{ g}$), which conformally attach on human skin without disturbing its contact. A stretchable composite electrode, which is formed by homogeneously intertwining silver nanowires (AgNWs) with thermoplastic polyurethane (TPU) nanofiber networks, is fabricated through synchronous electrospinning of TPU and electrospaying of AgNWs. Based on the triboelectrification effect, the open-circuit voltage, short-circuit current, and power density of the SI-TENG with a contact area of $2 \times 2 \text{ cm}^2$ and an applied force of 8 N can reach 95 V , $0.3 \mu\text{A}$, and 6 mW m^{-2} , respectively. By integrating the signal-processing circuits, the SI-TENG with excellent energy harvesting and self-powered sensing capability is demonstrated as a haptic sensor array to detect human actions. The SI-TENG exhibits extensive applications in the fields of human-machine interface and security systems.

1. Introduction

The rapid development of multifunctional wearable electronics has significantly facilitated our life.^[1–7] Among various kinds of smart electronics, stretchable sensors have received extensive applications in touch-sensor-based technologies, artificial intelligence systems, personal healthcare monitoring, and human-machine interfaces, due to their deformable and biocompatible characteristics.^[8,9] As a typical class of stretchable sensors, epidermal electronics require some special properties, including skin-like softness and texture, continuous working without frequent power change, and durability in harsh environments.^[10] These requirements have aroused people's desire to equip electronics with a stretchable, sustainable and light-weight power source. The triboelectric nanogenerator (TENG)^[11–18] is a promising alternative strategy to drive electronic systems by harvesting mechanical energy from ambient envi-

ronments.^[19–21] Moreover, it possesses self-powered sensing feature, which is widely used in multifunctional sensors due to its environmental friendliness, low cost, and universal material selection. Existing stretchable TENGs are usually fabricated from stretchable electrodes, which are realized by relatively complex crafts or structures, such as serpentine pattern (22%), interlocking kirigami (100%), and conductive polymer composites.^[22–24] As usual, conducting fillers, including carbon nanotubes, graphene, carbon paste, and silver nanowires, are embedded into elastomer substrates.^[25,26] Nevertheless, the percolated networks of conducting fillers cause some drawbacks. First, it is difficult to obtain electrodes from these approaches with both high stretchability and excellent electrical conductivity, because the conductivity usually drops rapidly or even disappears under high strain.^[27] Second, in order to achieve high conductivity, electrodes are usually designed to be thick, which to some extent affects the transparency, adhesion, and comfortability of the whole devices.^[28] To address these issues, a new class of stretchable and ultrathin electrode is required for next-generation skin-like TENGs.


Recently, considerable research efforts are dedicated to fabricating stretchable and ultrathin TENGs, which can adapt to

Y. Jiang, Prof. K. Dong, X. Li, J. An, X. Peng, J. Yi, C. Ning, R. Cheng, P. Yu, Prof. Z. L. Wang
Beijing Institute of Nanoenergy and Nanosystems
Chinese Academy of Sciences
Beijing 100083, P. R. China
E-mail: zlwang@gatech.edu

Y. Jiang, Prof. K. Dong, X. Li, J. An, X. Peng, J. Yi, C. Ning, R. Cheng, P. Yu, Prof. Z. L. Wang
School of Nanoscience and Technology
University of Chinese Academy of Sciences
Beijing 100049, P. R. China

D. Wu
Beijing Advanced Innovation Center for Materials Genome Engineering
Institute for Advanced Materials and Technology
University of Science and Technology Beijing
Beijing 100083, P. R. China

Prof. Z. L. Wang
School of Materials Science and Engineering
Georgia Institute of Technology
Atlanta, GA 30332-0245, USA

 The ORCID identification number(s) for the author(s) of this article can be found under <https://doi.org/10.1002/adfm.202005584>.

DOI: 10.1002/adfm.202005584

the deformation with human motion and reduce the discomfort induced by rigid interfaces.^[29,30] The stretchable TENGs still experience several challenges, including transparency, washability, high sensitivity, and long-term durability.^[31,32] However, due to the conducting fillers and complex structures, most stretchable TENGs with poor transparency have been reported,^[33] which impedes the direct visual access to the skin beneath the sensor.^[34] In addition, only a few studies have shown that the stretchable TENGs require exceptional water-resistance.^[35] Because those TENGs without a package is easy to be destroyed by water or vapor.^[36,37] Moreover, high sensitivity is important for a self-powered pressure sensor.²³ It is an effective method to modify the surface of sensors with regular patterns, such as pyramids, cubes, and lines, to improve their sensitivity.^[38,39] Besides, it is known that skin-like electronics require light-weight, but most of the stretchable TENGs fall short.^[40] Last but not least, it is difficult to simultaneously remain stable electrical properties and mechanical stretchability for most of the stretchable TENGs, because the percolated conductive networks of AgNWs are easy to break under high tensile strain.^[41] The stretchable and ultrathin TENGs are highly desirable for skin-like sensors and next-generation energy harvesters that are expected to be transparent, washable, highly sensitive, light-weight, and long-lasting.

In this paper, we present a simple and low-cost method for fabricating stretchable and ultrathin skin-inspired TENG (SI-TENG) with transparency, washability, and high-pressure sensitivity, which is used as skin-like self-powered haptic sensors. The excellent performances of the SI-TENG are attributed to the highly stretchable thermoplastic polyurethanes/silver nanowires (TPU/AgNWs) electrode, which is fabricated by electrospraying AgNWs intertwining with electrospinning TPU nanofiber networks. This structure provides the electrode with a high stretchability of 580% and a relatively stable resistance (from 5 to 732 Ω at a strain of 100%). More specifically, the composite electrode is further sandwiched between the top polydimethylsiloxane (PDMS) film and the bottom VHB tape. Based on the high stretchable and thin materials fabricated, the total thickness, weight, and stretchability of the SI-TENG are about 89 μm , 0.23 g, and 800%, respectively. The surface nanostructure modification of the PDMS film contributes to improving the surface charge density and enhancing pressure sensitivities (maximum pressure sensitivity of 9.973 mV Pa^{-1}). The developed SI-TENG with a valid contact area of 4 cm^2 could output the open-circuit voltage (V_{oc}) of 95 V and the short-circuit current (I_{sc}) of 0.3 μA , which is capable of lighting up more than 97 light-emitting diodes (LEDs). Furthermore, due to its high-pressure sensitivity, the SI-TENG acted as a game controller combines signal-processing circuits to provide a real-time haptic sensing signal. Our SI-TENG exhibited excellent mechanical properties, optical performances, and electronic performance compared with previous reported works, as shown in Table S1 of the Supporting Information. This work pushes the progress of TENGs for the applications in energy harvester and pressure sensing, which will shed light on the future development of self-powered wearable electronics and skin-like electronics.

2. Results and Discussion

2.1. Fabrication of the SI-TENG and Characterization

Figure 1a shows the basic structure of the single-electrode mode SI-TENG assembled by nanocomposite membranes. On the top side, a modified surface PDMS film is applied as the electrification layer, which generates triboelectric charges with external objects, owing to its good biocompatibility, superior mechanical properties, excellent flexibility/stretchability, and strong tendency to gain electrons. In the middle layer, AgNWs are distributed evenly throughout the TPU nanofiber network, which is adopted as the stretchable electrode, enabling the SI-TENG to operate stably under deformation. On the bottom side, a commercial VHB tap with outstanding mechanical and thermal properties serves as a structural supporting and protection layer. To further improve the performance of the SI-TENG, the surface of the PDMS film is modified with a vertically aligned microstructure, whose SEM image is shown in **Figure 1b**. Due to the increased frictional areas, the designed microstructure surface can extremely enhance the electricity output of the SI-TENG. The fabrication processes of the microstructure PDMS thin-film and the TPU/AgNWs electrode layer (whose SEM image shown in **Figure 1c**) are detailedly introduced in the Experimental Section. Since all of the materials for the SI-TENG are stretchable and thin, our SI-TENG achieves super stretchability along with arbitrary directions. Besides, these materials contribute to the thin thickness and light-weight of the whole devices, which are only 89 μm and 230 mg (area, 4 $\text{cm} \times 4 \text{ cm}$) (**Figure 1d**; **Figures S1a and S2**, Supporting Information). Furthermore, energy dispersive spectrometer analysis of the electrode and section for SI-TENG are shown in **Figures S3 and S4** of the Supporting Information.

The SI-TENG shows excellent optical transparency, which provides direct visual access to the skin beneath the sensor, and decreases the hurt produced by removing the sensor to detect the underlying skin (**Figure 1e**; **Figure S5**, Supporting Information). The SI-TENG forms a tight, comfortable, and conformal attachment to the natural skin and curved surface, as shown in **Figure 1f** and **Figure S1b** (Supporting Information). Due to a high level of attachment, the SI-TENG exhibited stable performance when being attached and pulled out with an object many times. In order to evaluate the mechanical properties of the SI-TENG, various kinds of complex mechanical deformations are conducted, including stretching, twisting, and bending (**Figure 1h–j**).

2.2. Working Mechanism

The working mechanism of the SI-TENG is concisely demonstrated in **Figure 2a**, which is in conjunction with triboelectrification and electrostatic induction. The SI-TENG will work in a single-electrode mode if the stretchable electrode is connected to the ground by a metal wire. When an active object (such as a glove, Kapton film, hand, or foot) contacts with the dielectric layer (PDMS thin film), the electrification process occurs at their interface and generates the same amount of charges with opposite polarities between the two contact surfaces. It is assumed that the active object is the dielectric material, such as Nylon film,

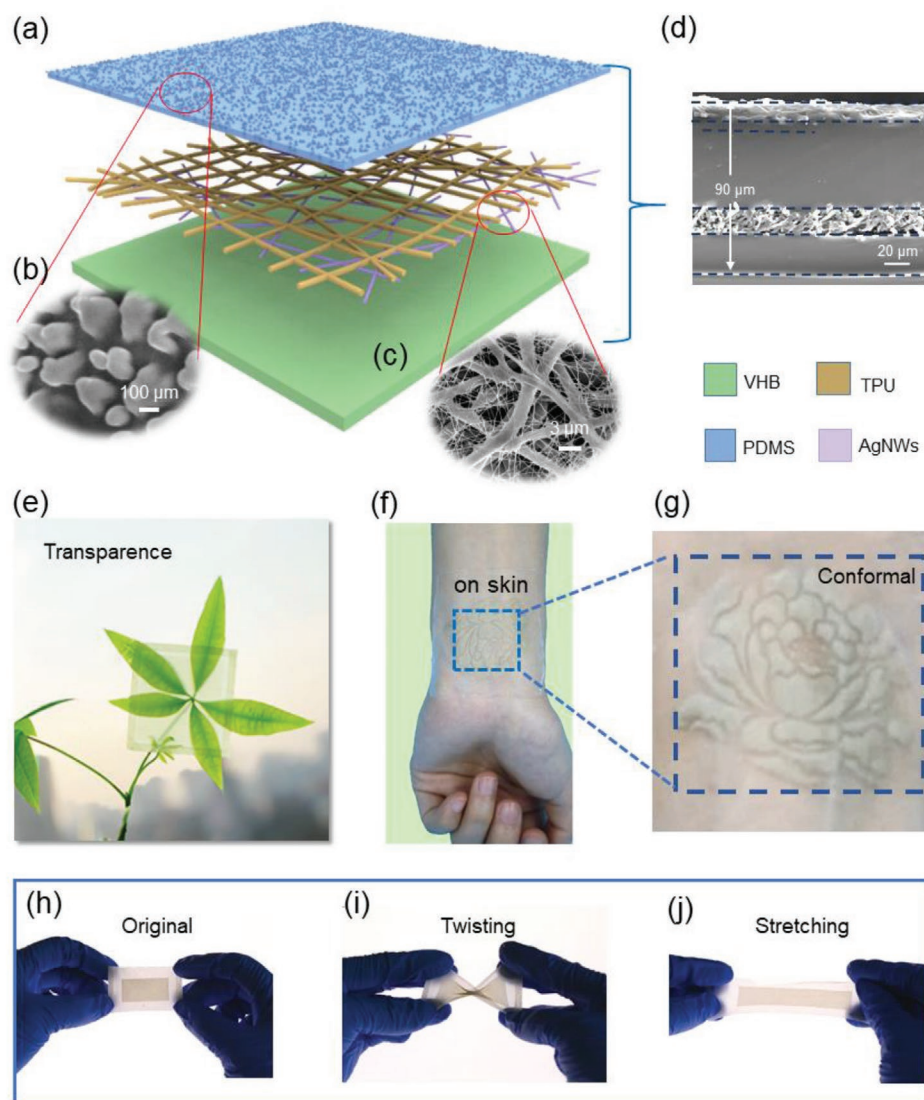


Figure 1. Structure design of the single-electrode ultrathin stretchable SI-TENG. a) Schematic diagram showing the detailed structure of the SI-TENG. b) SEM image of PDMS surface. c) SEM image of the TPU/AgNWs layer. d) Cross-section SEM image of the whole device. e) Optical image of the highly transparent SI-TENG. f.g) Optical images of SI-TENG attached on a skin. h–j) Optical images of twist and stretching of SI-TENG.

which produces more electrically positive in comparison with the PDMS film during the electrification process. With the contact of PDMS film surface and Nylon film, PDMS film gains negative triboelectric charges due to its more robust ability to capture negative charges, whereas the Nylon film will be positively charged. As the Nylon film begins to separate with the PDMS film, the potential difference will increase, resulting in instantaneous electron flow from the AgNWs electrode to the ground. The electron flowing continues until the Nylon film, and PDMS film is separated quietly far away. When the nylon film approaches to the PDMS film again, the electrons will flow back from the ground to the AgNWs electrode. Through the continuous contact and separation movements between the moving object and SI-TENG, an alternating current will be generated. Corresponding simulations of potential distributions of every component at the contact and separation states by COMSOL are shown in Figure 2b to observe the electricity generating process.

2.3. Electrical Output Performance

To characterize the electrical output performances of the SI-TENG, we use a linear motor to provide periodic contact–separation motion. The contact area is chosen as $20 \times 20 \text{ mm}^2$, the tapping force is applied as 8 N, and the maximum movement distance is set as 20 mm. In order to analyze the effect of the thickness of PDMS film on the output performance of the SI-TENG, several PDMS films with different thicknesses (25, 50, 100, 200, and 300 μm) are fabricated. The output performance of the V_{oc} , I_{sc} , and Q_{sc} increases first and then decreases with the increasing of the thickness of PDMS film (Figure 2c–e). It can be found that the thickness of PDMS film influences electrification and electric charge transformation. All the results demonstrate that the PDMS film with the thickness of 50 μm enables the SI-TENG the best electrical output performances (V_{oc} : 35 V, Q_{sc} : 13 nC, and I_{sc} : 0.08 μA). Theoretically,

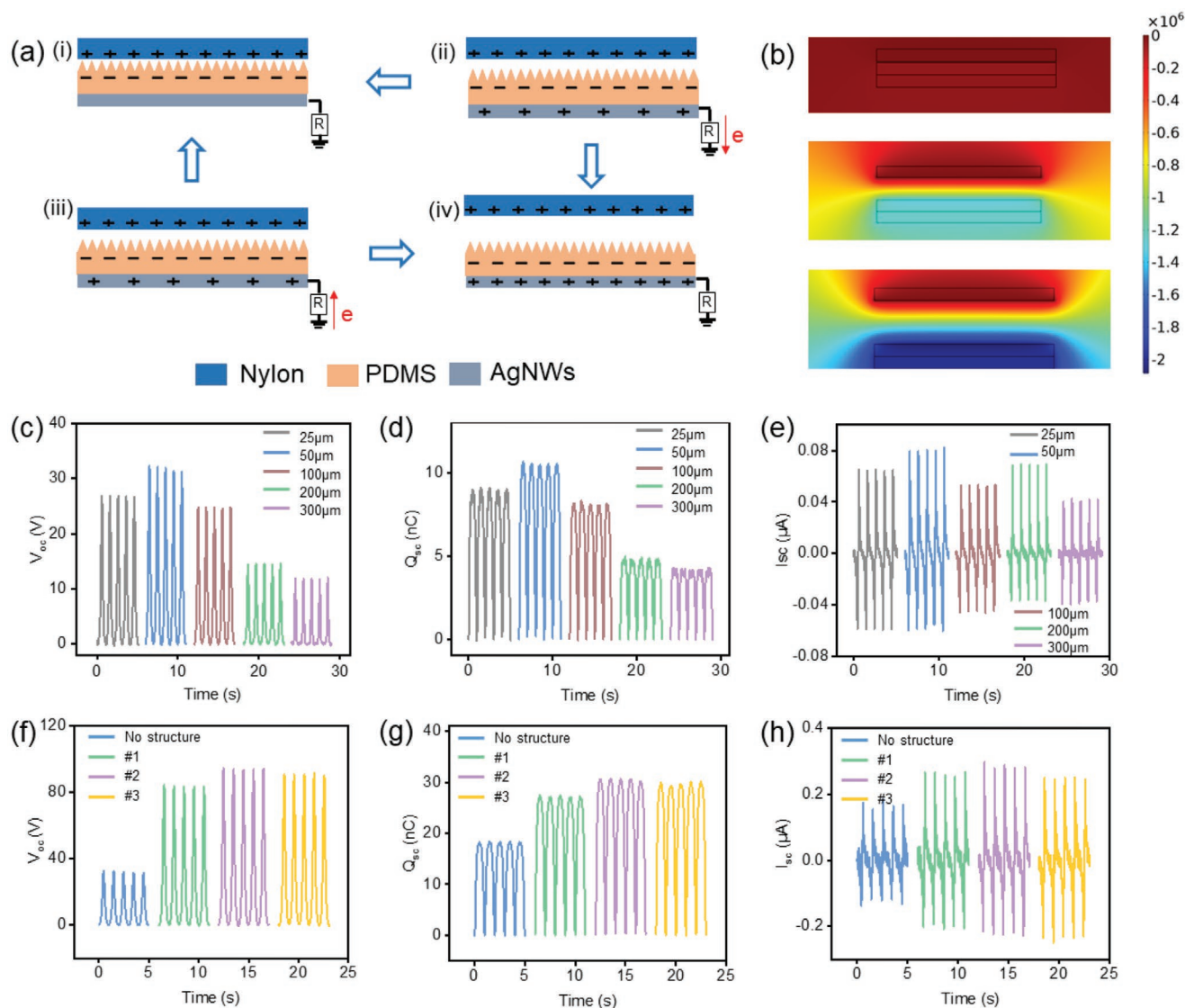


Figure 2. Working mechanisms and output performance of the SI-TENG in single-electrode mode. a) Schematics of the operating principle for the SI-TENG. b) Potential simulation by COMSOL to elucidate the working principle. c–e) Open-circuit voltage, short-circuit transferred charges, and short-circuit current of different thicknesses of the electrification layer for the SI-TENG. f–h) Open-circuit voltage, short-circuit transferred charges, and short-circuit current of different microstructure surfaces of the electrification layer for the SI-TENG. (#1 thickness of Ti mask is 1 nm, #2 thickness of Ti mask is 3 nm, and #3 thickness of Ti mask is 5 nm.)

the thickness of PDMS film in the proper region contributes to electric charge transformation, but thin PDMS film reduces the electrification ability. As a result, the PDMS film with the thickness of 50 μm was chosen to fabricate the SI-TENG.

To clarify the effect of surface micromorphology on the electrical performance, SI-TENGs with several kinds of dielectric layers are fabricated. It is found that the sticky surface of PDMS film impairs the process of contact–separation, leading to the decreasing of the output. To further improve the output performance of the SI-TENG, we modify the surface of PDMS film with inductively coupled plasma (ICP) reactive ion etching after Ti mask is treated by physical vapor deposition. Besides, to obtain different surface roughness of the PDMS film, Ti sputter coaters with varying thicknesses are used. Figure 6 of the Supporting Information depicts that the SEM image of different

thickness of Ti sputter coater presents different microstructures. The electrical output of the SI-TENG fabricated by various-rough surface PDMS is shown and compared in Figure 2f–h (#1 thickness of Ti mask is 1 nm, #2 thickness of Ti mask is 3 nm, and #3 thickness of Ti mask is 5 nm). Through modification based on nanowire-structural surface, these SI-TENGs show better electrical output capabilities than the SI-TENG with no nanostructure, demonstrating that the modified surface enormously enhances the triboelectrification. It is depicted that the output performance first increases and then decreases as the thickness of the mask increases. The result demonstrates that proper surface roughness increases the contact area, while the surface with dense nanowires diminishes the contact area. As indicated above, the SI-TENG modified with ICP etching by the 3 nm thickness of Ti mask obtains the highest output.

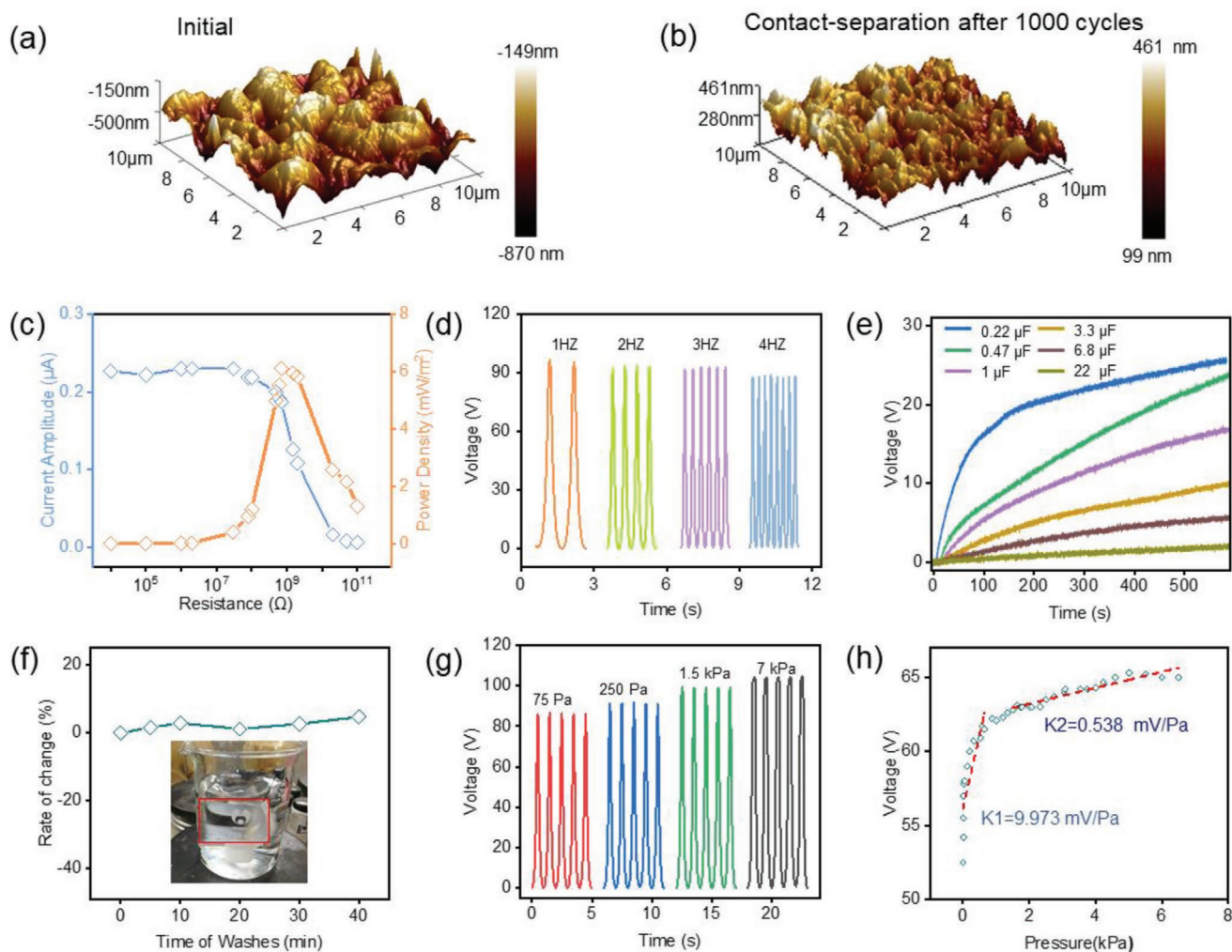


Figure 3. Electrical output, stability, and sensitivity of the SI-TENG. a,b) AFM image of surface change for contact–separation 1000 cycles. c) Dependence of the output current and peak power on load resistance. d) The open-circuit voltage of SI-TENG at various applied frequencies (1–4 Hz). e) Charging curve of the SI-TENG at various capacitance capacity. f) The output voltage of the SI-TENG under different washing time. g) The output voltage of the SI-TENG under different pressures. h) The output voltage of the SI-TENG as a function of applied pressure.

To characterize the working stability of the SI-TENG, we utilize the atomic force microscopy (AFM) to analyze the surface morphology. **Figure 3a,b** shows the rough surface morphologies of the SI-TENG before and after tapping. It is indicated that no visible tip damage is observed after tapping 1000 cycles. This result corresponds well with the previous reports, indicating that the SI-TENG would durably operate due to the high durability of microstructures. Besides, the output of the SI-TENG remained consistent without degradation after 40 000 cycles of tapping tests with the loading pressure of 5 kPa at a frequency of 1 Hz, as shown in Figure S7 of the Supporting Information.

To evaluate the effective output performance of the SI-TENG, we measure its output voltage under different resistances. With the increase of the external resistances, the maximum output current of SI-TENG drops. At the same time, instantaneous power density is maximized at a load resistance of 840 M Ω , corresponding to a peak power density of 6.1 mW m $^{-2}$, as shown in Figure 3c. Movies S1 and S2 of the Supporting Information demonstrate that the SI-TENG attached to curve objects (including beaker or arms) could light up 97 LEDs in series through tapping. The output

performance of the SI-TENG under different frequencies is also investigated, and there are no noticeable output changes with the loading frequencies varied from 1 to 4 Hz (Figure 3d). Furthermore, the harvested electricity can be rectified and stored in capacitors or batteries for later use. The charging ability of the SI-TENG under different capacitors is shown in Figure 3e, demonstrating that the charging speed accelerates by the capacitance reducing. Stored electricity in a capacitor could maintain in sustainably powering wearable electronics. From these analyses, it is found that developed SI-TENG is likely to be used as a potential power source.

2.4. Washability and Sensing Characterization

As skin-like electronics, washability is very important for long-term and repeated usage. To evaluate the washability of the SI-TENG, the output voltages under various washing times (from 10 to 40 min) are examined, as shown in Figure 3h and Figure S8 (Supporting Information). It can be found that no apparent variation of the output voltage is observed throughout

the washing tests. Considering the constant voltage output against machine washing, our SI-TENG is the potential for widespread application in daily life.

Due to excellent pressure sensing performance, the SI-TENG shows potential applications in self-powered human-machine interactive devices. We utilize a linear motor to provide a precisely controlled reciprocating motion to generate repetitive contact-separation processes. Figure 3g illustrates that the output voltage signal with a square-wave shape is uniform and repeatable when the applied pressure is kept as constant. As the contact force increases, the corresponding voltage signal output also increases and finally saturates at 65 V when the applied pressure approaches to 6 KPa (Figure 3h). The result can be attributed to that the increased applied pressure contributes to more contact areas. The enhanced contact areas can increase the surface charge density, resulting in higher voltage output. It should be noted that the curve exhibits two distinct regions. In the low-pressure region (0–1.6 KPa), the SI-TENG

shows a well-behaved linear response with the pressure sensitivity of 9.973 mV Pa^{-1} , while in the high-pressure region ($>1.6 \text{ KPa}$), the pressure sensitivity is 0.538 mV Pa^{-1} . The two-region pressure linear response behavior is due to the enhancement effect of the contact surface. The increment-real-contact area, in response to an increase of pressure, is much more in the low-pressure region than that in the high-pressure region. As a result, the SI-TENG exhibits a more sensitive response in the low-pressure region ($<1.6 \text{ KPa}$).

2.5. Stretchability Characterization

For skin-like sensors, high stretchability is an essential basic requirement for their extensive applications. The high stretchability of SI-TENG, including the electrical outputs and mechanical performance under the tensile state, is further investigated. Figure 4a shows that SI-TENG was uniaxially stretched to

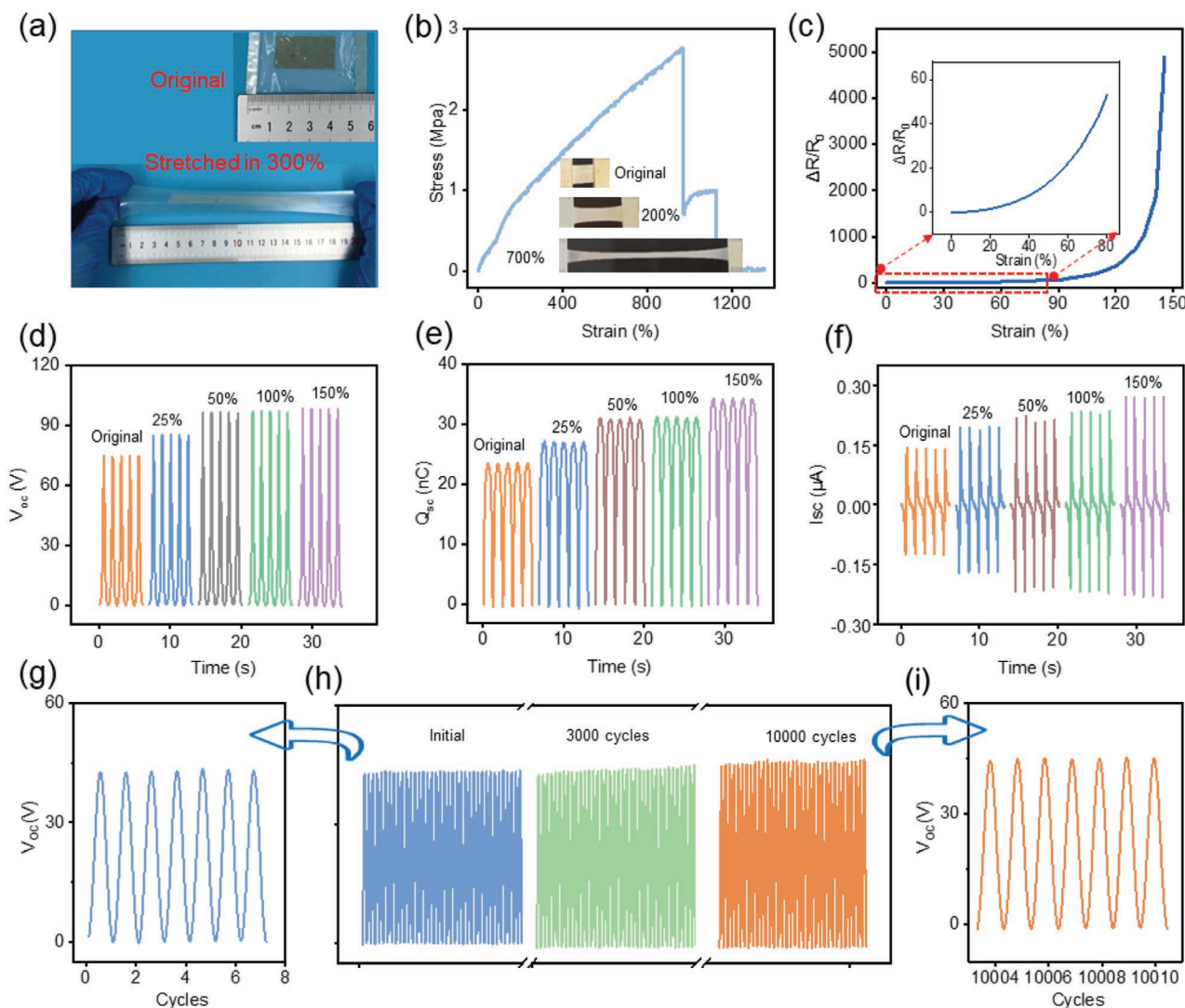


Figure 4. Electrical and mechanical characterization of the SI-TENG under stretching state. a) The strain–stress of the composite electrode and the SI-TENG. b) The strain–stress of SI-TENG. c) Resistance variation of the composite electrodes under different tensile strains. d–f) The output performance of the SI-TENG under different tensile strains. g–i) The output voltage of the SI-TENG under long time tensile loading cycle.

200% compared with the original length, presenting excellent mechanical properties. The tensile strain capacity of the SI-TENG and the composite electrode are tested with a stress-strain gauge by precise length control (Figure 4b; Figure S9a, Supporting Information). This structure provides the electrode with a high stretchability (580%) and a relatively stable resistance (from 5 to 732 Ω at a strain of 100%), as shown in Figure S9a,b of the Supporting Information. The resistance changes of the electrode under strain are compared with other electrodes in Figure S10 of the Supporting Information. In detail, the SI-TENG shows a failure strain of 800% under the ultimate stress of 2.8 MPa, which is attributed to the tight multilayer composite structure. Besides, owing to the low Young's modulus, VHB layer ruptures at a strain of 1200%. Furthermore, the electrode exhibits good robustness of the resistance under repeated stretching cycles as shown in Figure S11 of the Supporting Information, as well as the excellent flexibility of the SI-TENG as shown in Figure S12 of the Supporting Information.

To further study the conductivity of the SI-TENG, the uniaxial tensile test is conducted. As shown in Figure 4c, the resistance of the composite electrode increases with the elongation of the SI-TENG. Due to the high internal impedance of the SI-TENG, the slight increase of the resistance (from 5 to 732 Ω at the strain of 100%) is acceptable, which has little negative impacts on the performance of the SI-TENG.

In virtue of the excellent stretchability of the SI-TENG, it is interesting to explore its electrical outputs under the stretched states. Figure 4d–f shows the output performance of the SI-TENG with the contact area of 1 cm \times 2 cm under different stretched states. The result shows that the output performance increases with the increasing of tensile strains from 0% to 150%, including the V_{oc} (80 V to 110 V), Q_{sc} (22 to 35 nC), and I_{sc} (0.15 to 0.3 μ A). The reason can be attributed to an increased contact area between PDMS film and the external substrate. The stretchability is almost inevitable for the SI-TENG. As shown in Figure 4g–i, the output voltage has no noticeable change under the continuous operation of 100 000 cycles at the tensile strain of 30%, confirming the superior stretchability of our SI-TENG.

2.6. Application of Skin-Like Haptic Sensor

With the arrival of the fourth industrial revolution, wearable electronics must be portable and compatible with wearable systems. To meet these requirements, an ultrastretchable game controller with transparent, flexible, conformable, and self-powered features is designed. Figure 5a schematically illustrates the structure of the game controller, which consists of 3 \times 3 array. As shown in Figure 5b, the self-powered game controller consists of 9 sensing units with the 3 \times 3 array, including PDMS electrification layer, TPU/AgNWs electrode layer, VHB insulating layer, TPU/AgNWs shielding layer, and VHB/TPU substrate layer. Once contacting with other materials, the modified PDMS film tends to gain negative triboelectric charges and promotes touch sensitivity. Figure S13 of the Supporting Information illustrates the output voltage of the haptic sensor as a function of applied pressure and the strain–stress curve of the haptic sensor is shown in Figure S14 of the Supporting Information. In practical usage, it is vital for sensing that the

corresponding signals are independently generated from each sensing unit. The optimized structure is specially designed to remove the interference of low-frequency noise from the ambient environment, in order to detect the voltage signal precisely. The electrode layer is made of individual units of circle line in columns, and every unit is around by a hollow circle (TPU/AgNWs thin-film) as a shield layer, which can reduce the electrostatic interference. Between the electrode layer and substrate layer, a shielding layer made of TPU/AgNWs thin-film eliminates the electrostatic induction from electrode layers and the environment. Another merit of the haptic sensor is its conformability to work on curved surfaces, such as a human hand (Figure 5c). For practical applications, a sensing system of a skin-like game controller was developed through integrating the SI-TENG with a signal-processing circuit. As displayed in Figure 5d, the game controller system consists of three major parts, an SI-TENG with 3 \times 3 sensing array, a signal processing circuit, and a Labview program-based computer. Once a finger gently touched the sensor, the distinct output voltage processes in response to the mechanical agitation. Through the analog-to-digital (A/D) converter, the voltage signal is converted into a digital signal, which further triggers the multicontrol unit. After signal filtering and converting processing, real-time results can be displayed in the designed program, which controls character movement in games. Figure 5e and Movie S3 (Supporting Information) shows the self-powered skin-like game controller system. The enlarged real-time voltage signals of all the channels are shown in Figure 5f. The corresponding output voltage signals with a time of each channel are shown in Figure 5g, indicating the feasibility of our sensing system. Therefore, the self-powered skin-like game controller developed here shows the potential in a variety of areas, including automatic control, human–machine interface, remote operation, and security systems.

3. Conclusion

In summary, based on the TPU fibrous and AgNWs electrode, we designed a stretchable, ultrathin, washable, and highly sensitive SI-TENG, which can achieve a strain of 800% and a total thickness of about 89 μ m. The top surface of the SI-TENG is modified with vertically aligned microstructure by plasma treatment. The bottom surface is super adhesive, which allows the SI-TENG to attach to various curved objects. Under the applied force of 8 N and the loading frequency of 1 Hz, the V_{oc} and I_{sc} can reach 95 V and 0.3 μ A, respectively, while the optimized external resistance is 840 M Ω . In addition, the SI-TENG shows a constant output resistant to water. The high transmittance (50%) is of paramount significance for a skin-like sensor, which enables the sensor visible for powering wearable electronics. In addition, the SI-TENG has achieved an ultrahigh level of pressure sensitivity in an extremely low-pressure region. Based on the advantages of the SI-TENG, a self-powered skin-like game controller has been designed and demonstrated. Considering that the SI-TENG features other significant advantages in thickness, stretchability, washability, and pressure-sensitivity, it has a promising prospect for the self-powered sensory system or as the energy supplier for the next-generation wearable electronics.

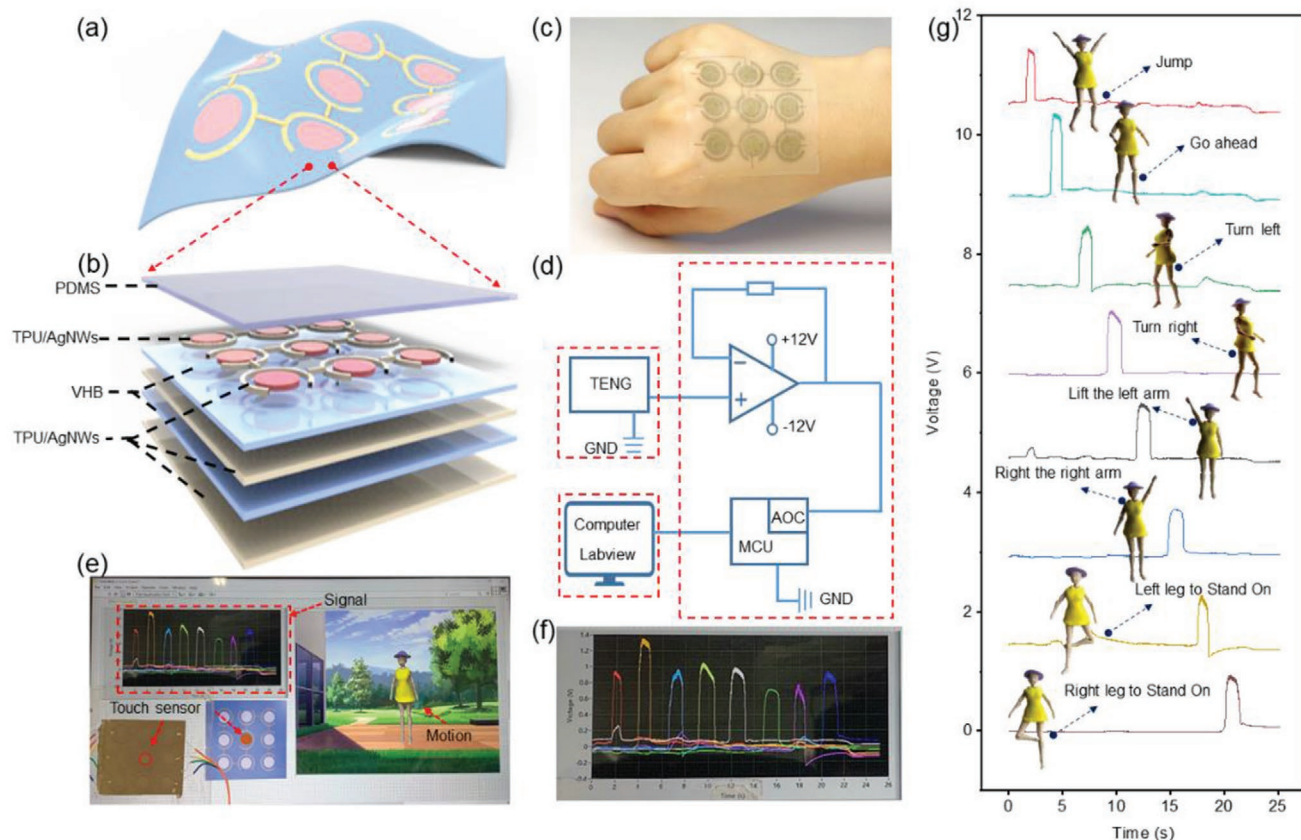


Figure 5. Demonstration of the developed SI-TENG as a haptic sensor for amusement games. a) Scheme diagram of the 3×3 SI-TENG array. b) Structure of the 3×3 SI-TENG array. c) Picture showing that the SI-TENG is attached on the hand. d) Electric circuit diagram of the sensing system. e) Demonstration showing that the SI-TENG array control game character movements. f) Screenshot showing the real-time output voltage. g) Voltage output signals of the 3×3 SI-TENG array.

4. Experimental Section

Fabrication of the Microstructure PDMS Thin Film: A layer of PDMS film was prepared, whose thickness was about $50 \mu\text{m}$. Then, a layer of Ti with the thickness of 3 nm was sputtered on the PDMS film with a sputter coater as an etching mask. Subsequently, the sample was etched by means of reactive ion etching (ICP) for 120 s. During the reaction, Ar, O_2 , and CF_4 gases were introduced into the ICP chamber at flow rates of 15.0, 10.0, and 30.0 sccm , respectively. The pressure was set as 15 mTorr. And the 400 W power was used to generate high-density plasma and accelerate plasma ions toward the PDMS surface. The etching time was 120 s.

Fabrication of the Stretchable Composite Electrode: The precursor of polyurethane nanofibers was dissolved TPU particles (1180, Aladdin) into hexafluoroisopropanol (Aladdin, 4 wt%) and stirred with a magnetic spinor for 3 h at room temperature. The silver nanowires dispersion of 10 mg mL^{-1} was diluted with alcohol to 1 mg mL^{-1} . Then, the TPU solution and silver nanowires dispersion were separately fixed onto a shared syringe pump. The electrospinning process was conducted at a positive voltage of 15 kV and a negative voltage of 2.5 kV, through an electrospinning device (Ucalery, ET-2535H). The distance between the needles for the TPU solution and silver nanowires dispersion was 3 cm. In the fabrication process, the needle-collector distance was set to be 12 cm. The pump rates for the TPU electrospinning and silver nanowires electrospinning were set to be 0.2 and 1.2 mm min^{-1} , respectively. The Ag NWs/TPU films were collected on the aluminum foil wrapping around a revolving roller.

Fabrication of the SI-TENG: The SI-TENG consists of three layers. On the bottom side, a layer of TPU ($2 \text{ cm} \times 2 \text{ cm}$) with a thickness of $5 \mu\text{m}$ serves as a substrate. then, a layer of commercial VHB tap ($2 \text{ cm} \times 2 \text{ cm}$)

with a thickness of $10 \mu\text{m}$ was firmly stick to the TPU film, as a structural supporting and protection layer. A TPU/AgNWs film with a thickness of $15 \mu\text{m}$ was pasted on the substrate. On the top side, a microstructure PDMS film with a thickness of $50 \mu\text{m}$ adhered to the electrode as the electrification layer.

Characterization and Measurement: A Nova 250 SEM was used to measure the surface morphology of microstructure PDMS, TPU/AgNWs layer, and the section SEM image of the whole device. A step motor (LinMot E1100) was applied to provide the periodic contact-separation movement for TENGs. A programmable electrometer (Keithley, model 6514) was adopted to test the open-circuit voltage, short-circuit current, and transferred charge. The software platform was constructed based on LabView, which was capable of realizing real-time data acquisition.

Supporting Information

Supporting Information is available from the Wiley Online Library or from the author.

Acknowledgements

Y.J., K.D., X.L. contributed equally to this work. The authors are grateful for the support received from the National Key R&D Project from Minister of Science and Technology (Grant No. 2016YFA0202704), the

Shanghai Sailing Program (Grant No. 19S28101), and the Fundamental Research Funds for the Central Universities (Grant No. 19D128102). Informed consent was obtained from the volunteers who participated in the experiments.

Conflict of Interest

The authors declare no conflict of interest.

Keywords

electronic skins, flexible electronics, haptic sensors, self-powered, triboelectric nanogenerators

Received: July 3, 2020

Revised: August 6, 2020

Published online:

- [1] J. Wang, S. Li, F. Yi, Y. Zi, J. Lin, X. Wang, Y. Xu, Z. L. Wang, *Nat. Commun.* **2016**, 7, 12744.
- [2] H. U. Chung, B. H. Kim, J. Y. Lee, J. Lee, Z. Xie, E. M. Ibler, K. Lee, A. Banks, J. Y. Jeong, J. Kim, C. Ogle, D. Grande, Y. Yu, H. Jang, P. Assem, D. Ryu, J. W. Kwak, M. Namkoong, J. B. Park, Y. Lee, D. H. Kim, A. Ryu, J. Jeong, K. You, B. Ji, Z. Liu, Q. Huo, X. Feng, Y. Deng, Y. Xu, K. I. Jang, J. Kim, Y. Zhang, R. Ghaffari, C. M. Rand, M. Schau, A. Hamvas, D. E. Weese-Mayer, Y. Huang, S. M. Lee, C. H. Lee, N. R. Shanbhag, A. S. Paller, S. Xu, J. A. Rogers, *Science* **2019**, 363, 0780.
- [3] X. Peng, K. Dong, C. Y. Ye, Y. Jiang, S. Y. Zhai, R. W. Cheng, D. Liu, X. P. Gao, J. Wang, Z. L. Wang, *Sci. Adv.* **2020**, 6, 9624.
- [4] C. Wang, C. Wang, Z. Huang, S. Xu, *Adv. Mater.* **2018**, 30, 1801368.
- [5] S. Choi, H. Lee, R. Ghaffari, T. Hyeon, D. H. Kim, *Adv. Mater.* **2016**, 28, 4203.
- [6] H. Chen, Y. Song, X. Cheng, H. Zhang, *Nano Energy* **2019**, 56, 252.
- [7] K. Dong, J. Deng, Y. Zi, Y. C. Wang, C. Xu, H. Zou, W. Ding, Y. Dai, B. Gu, B. Sun, Z. L. Wang, *Adv. Mater.* **2017**, 29, 1702648.
- [8] K. Dong, Z. Wu, J. Deng, A. C. Wang, H. Zou, C. Chen, D. Hu, B. Gu, B. Sun, Z. L. Wang, *Adv. Mater.* **2018**, 30, 1804944.
- [9] J. Lee, B. Llerena Zambrano, J. Woo, K. Yoon, T. Lee, *Adv. Mater.* **2020**, 32, 1902532.
- [10] X. Wang, Y. Gu, Z. Xiong, Z. Cui, T. Zhang, *Adv. Mater.* **2014**, 26, 1336.
- [11] X.-S. Zhang, M.-D. Han, R.-X. Wang, B. Meng, F.-Y. Zhu, X.-M. Sun, W. Hu, W. Wang, Z.-H. Li, H.-X. Zhang, *Nano Energy* **2014**, 4, 123.
- [12] K. Dong, X. Peng, J. An, A. C. Wang, J. Luo, B. Sun, J. Wang, Z. L. Wang, *Nat. Commun.* **2020**, 11, 2868.
- [13] H. Zou, L. Guo, H. Xue, Y. Zhang, X. Shen, X. Liu, P. Wang, X. He, G. Dai, P. Jiang, H. Zheng, B. Zhang, C. Xu, Z. L. Wang, *Nat. Commun.* **2020**, 11, 2093.
- [14] C. Xu, Y. Zi, A. C. Wang, H. Zou, Y. Dai, X. He, P. Wang, Y. C. Wang, P. Feng, D. Li, Z. L. Wang, *Adv. Mater.* **2018**, 30, 1706790.
- [15] C. Xu, B. Zhang, A. C. Wang, H. Zou, G. Liu, W. Ding, C. Wu, M. Ma, P. Feng, Z. Lin, Z. L. Wang, *ACS Nano* **2019**, 13, 2034.
- [16] S. Lin, L. Xu, C. Xu, X. Chen, A. C. Wang, B. Zhang, P. Lin, Y. Yang, H. Zhao, Z. L. Wang, *Adv. Mater.* **2019**, 31, 1808197.
- [17] J. Nie, Z. Wang, Z. Ren, S. Li, X. Chen, Z. Lin Wang, *Nat. Commun.* **2019**, 10, 2264.
- [18] Z. L. Wang, *Nano Energy* **2020**, 68, 104272.
- [19] J. Chen, H. Guo, J. Zheng, Y. Huang, G. Liu, C. Hu, Z. L. Wang, *ACS Nano* **2016**, 10, 8104.
- [20] K. Dong, X. Peng, Z. L. Wang, *Adv. Mater.* **2020**, 32, 1902549.
- [21] H. Wu, Z. Su, M. Shi, L. Miao, Y. Song, H. Chen, M. Han, H. Zhang, *Adv. Funct. Mater.* **2018**, 28, 1704641.
- [22] K. Parida, G. Thangavel, G. Cai, X. Zhou, S. Park, J. Xiong, P. S. Lee, *Nat. Commun.* **2019**, 10, 2158.
- [23] X. Yu, J. Pan, J. Zhang, H. Sun, S. He, L. Qiu, H. Lou, X. Sun, H. Peng, *J. Mater. Chem. A* **2017**, 5, 6032.
- [24] J. Shi, X. Chen, G. Li, N. Sun, H. Jiang, D. Bao, L. Xie, M. Peng, Y. Liu, Z. Wen, X. Sun, *Nanoscale* **2019**, 11, 7513.
- [25] J. Y. Oh, S. Rondeau-Gagne, Y. C. Chiu, A. Chortos, F. Lissel, G. N. Wang, B. C. Schroeder, T. Kurosawa, J. Lopez, T. Katsumata, J. Xu, C. Zhu, X. Gu, W. G. Bae, Y. Kim, L. Jin, J. W. Chung, J. B. Tok, Z. Bao, *Nature* **2016**, 539, 411.
- [26] W. Liu, M. S. Song, B. Kong, Y. Cui, *Adv. Mater.* **2017**, 29, 1603436.
- [27] H. Wu, Y. Huang, F. Xu, Y. Duan, Z. Yin, *Adv. Mater.* **2016**, 28, 9881.
- [28] X. Chen, Y. Wu, J. Shao, T. Jiang, A. Yu, L. Xu, Z. L. Wang, *Small* **2017**, 13, 1702929.
- [29] S. Park, H. Kim, M. Vosgueritchian, S. Cheon, H. Kim, J. H. Koo, T. R. Kim, S. Lee, G. Schwartz, H. Chang, Z. Bao, *Adv. Mater.* **2014**, 26, 7324.
- [30] C. Pang, J. H. Koo, A. Nguyen, J. M. Caves, M. G. Kim, A. Chortos, K. Kim, P. J. Wang, J. B. Tok, Z. Bao, *Adv. Mater.* **2015**, 27, 634.
- [31] G. A. Salvatore, N. Munzenrieder, T. Kinkeldei, L. Petti, C. Zysset, I. Strebel, L. Buthe, G. Troster, *Nat. Commun.* **2014**, 5, 2982.
- [32] S. Yao, Y. Zhu, *Adv. Mater.* **2015**, 27, 1480.
- [33] J. Mu, C. Hou, G. Wang, X. Wang, Q. Zhang, Y. Li, H. Wang, M. Zhu, *Adv. Mater.* **2016**, 28, 9491.
- [34] T. Q. Trung, N. E. Lee, *Adv. Mater.* **2016**, 28, 4338.
- [35] K. Dong, Y. C. Wang, J. Deng, Y. Dai, S. L. Zhang, H. Zou, B. Gu, B. Sun, Z. L. Wang, *ACS Nano* **2017**, 11, 9490.
- [36] H. Guo, Z. Wen, Y. Zi, M.-H. Yeh, J. Wang, L. Zhu, C. Hu, Z. L. Wang, *Adv. Energy Mater.* **2016**, 6, 1501593.
- [37] Y. Zou, P. Tan, B. Shi, H. Ouyang, D. Jiang, Z. Liu, H. Li, M. Yu, C. Wang, X. Qu, L. Zhao, Y. Fan, Z. L. Wang, Z. Li, *Nat. Commun.* **2019**, 10, 2695.
- [38] L. Zhao, H. Li, J. Meng, A. C. Wang, P. Tan, Y. Zou, Z. Yuan, J. Lu, C. Pan, Y. Fan, Y. Zhang, Y. Zhang, Z. L. Wang, Z. Li, *Adv. Funct. Mater.* **2020**, 30, 1907999.
- [39] C. Zhang, S. Liu, X. Huang, W. Guo, Y. Li, H. Wu, *Nano Energy* **2019**, 62, 164.
- [40] Z. Feng, S. Yang, S. Jia, Y. Zhang, S. Jiang, L. Yu, R. Li, G. Song, A. Wang, T. Martin, L. Zuo, X. Jia, *Nano Energy* **2020**, 74, 104805.
- [41] Y. Liu, M. Pharr, G. A. Salvatore, *ACS Nano* **2017**, 11, 9614.